

Unrestrained Molecular Dynamics of Photodamaged DNA in Aqueous Solution

Tami I. Spector,[†] Thomas E. Cheatham III, and Peter A. Kollman^{*‡}

Contribution from the Department of Pharmaceutical Chemistry, University of California, San Francisco, California 94143-0446, and Department of Chemistry, University of San Francisco, San Francisco, California 94117-1080

Received December 20, 1996. Revised Manuscript Received May 8, 1997[⊗]

Abstract: The structural impact of photolesions on DNA was investigated by carrying out molecular dynamics simulations of the T5/T6 cis-syn dimer (**A**), T5/T6 6-4 adduct (**B**), and native decamer (**C**) of d(CGATTACGC)₂. For the cis-syn dimer containing decamer the simulations provided a structure very similar to that derived with experimental NOE data. Specifically, distortions of the simulated cis-syn dimer duplex (**A**) were primarily localized at the lesion site and had an overall bend similar to that of the refined NMR structure. For the simulated 6-4 adduct duplex (**B**), although there was considerable coincidence with the NMR derived structure, an intact hydrogen bond/dipole–dipole interaction between the T6 pyrimidone carbonyl oxygen and A15/NH₂ was observed, which was not found in the NMR derived structure. This hydrogen bond leads to a structure that seems to better account for some of the unusual experimental NOEs than the refined NMR structure. In addition, for the 6-4 adduct (**B**), the overall bend was significantly smaller than that suggested by the NMR derived structure. This difference in overall bend is presumably a result of differences in the torsion angles at the lesion site for the simulated vs the experimental structure. Overall these simulations agreed well with the features of the spectroscopically determined structures and reveal the power of molecular dynamics methods with explicit solvation and accurate representation of long-range electrostatic interactions to usefully model noncanonical forms of DNA.

Introduction

Complete characterization of the molecular structures, genes,¹ and cellular repair mechanisms associated with UV-damaged DNA should ultimately lead to the effective clinical treatment of skin cancer.² Toward this goal scientists have identified the cis-syn cyclobutane dimer and 6-4 adduct formed at adjacent pyrimidine sites as the most mutagenic and carcinogenic lesions produced by UV irradiation of DNA.³ More recently, spectroscopic studies of these photoproducts have begun to reveal the relationship between the structure of a DNA oligomer with a cis-syn or 6-4 dithymidine lesion and its potential carcinogenicity. These studies include the NMR determination of the structure of the cis-syn dimer containing dodecamer d(CGTAT-TATGC)₂⁴ and the cis-syn dimer and 6-4 adduct of d(CGAT-TACGC)₂.⁵ These NMR analyses, along with the recent X-ray determination of the structure of a cyclobutane pyrimidine dimer DNA duplex/T4-endonuclease V complex,⁶ are leading to a greater understanding of the mechanism of mutagenesis and enzymatic repair of photodamaged DNA.

To date, enlightening theoretical investigations of photodamaged DNA have been limited by the available computational methods and the high cost of simulating large, highly charged aqueous oligonucleotides. Due to these limitations, primarily in vacuo energy minimization studies of photodamaged oligo-

nucleotides have been reported previously. Specifically, Rao *et al.*⁷ and Pearlman and Kim⁸ both examined the Dickerson dodecamer d(CGCGAATTCGCG)₂⁹ with a cis-syn dimer at the T-T sites. These studies yielded local deformations at the cis-syn lesion which were qualitatively similar, but provided vastly different overall helical bends. Thus, Rao *et al.* reported a small bend of 7°, whereas Pearlman and Kim found a 44° overall bend. Presumably, the different methods used to model build the initial photodamaged structures used for these in vacuo optimizations lead to the conflicting overall bend values. Alderfer *et al.* has also computationally studied cis-syn lesion containing polyA–polyT hexamers and dodecamers via in vacuo minimization.¹⁰

Recently Cheatham and Kollman demonstrated that molecular dynamics (MD) using the Cornell *et al.*¹⁵ force field with the particle mesh Ewald (PME) code accurately simulates A-DNA to B-DNA transitions at constant pressure with realistic charge and solvent conditions.¹¹ While this study was in progress, Miaskiewicz *et al.*, using the methodology of Cheatham and Kollman,¹¹ reported the first MD (with PME) simulation on the cis-syn containing DNA oligomer d(CGCGAATTCGCG)₂.¹² In agreement with Rao *et al.*'s earlier in vacuo structure, this simulation also yielded a lesion containing structure with a small overall curvature of 10° relative to the native dodecamer. Using these same methods we report here simulations on a cis-syn dimer with a sequence different from that studied by Mi-

* To whom correspondence should be addressed.

[†] University of San Francisco.

[‡] University of California, San Francisco.

[⊗] Abstract published in *Advance ACS Abstracts*, July 1, 1997.

(1) Leffell, D. J.; Brash, D. E. *Sci. Am.* **1996**, 52–59.

(2) Carell, T. *Angew. Chem., Int. Ed. Engl.* **1995**, 34, 2491–2494.

(3) Taylor, J-S. *Pure Appl. Chem.* **1995**, 67, 183–190.

(4) Taylor, J-S.; Garrett, D. S.; Brockie, I. R.; Svoboda, D. L.; Telser, J. *Biochemistry* **1990**, 29, 8858–8866.

(5) Kim, J-K; Patel, D.; Choi, B-S. *Photochem. Photobiol.* **1995**, 62, 44–50.

(6) Vassilyev, D. G.; Kashiwagi, T.; Mikami, Y.; Ariyoshi, M.; Iwai, S.; Ohtsuka, E.; Morikawa, K. *Cell* **1995**, 83, 773–782.

(7) Rao, S. N.; Keepers, J. W.; Kollman, P. A. *Nucleic Acids Res.* **1984**, 12, 4789–4807.

(8) Pearlman, D. A.; Holbrook, S. R.; Pirkle, D. H.; Kim, S-H. *Science* **1985**, 227, 1304–1308.

(9) Dickerson, R. E.; Drew, H. R.; Conner, B. N.; Wing, R. M.; Fratini, A. V.; Kopka, M. L. *Science* **1982**, 216, 475–485.

(10) Alderfer, J. L.; G. Raghunathan, G.; Kieber-Emmons, T.; Rein, R. *J. Biomol. Struct. Dyn.* **1990**, 7, 899–913.

(11) Cheatham, T. E.; Kollman, P. A. *J. Mol. Biol.* **1996**, 259.

(12) Miaskiewicz, K.; Miller, J.; Cooney, M.; Osman, R. *J. Am. Chem. Soc.* **1996**, 118, 9156–9163.

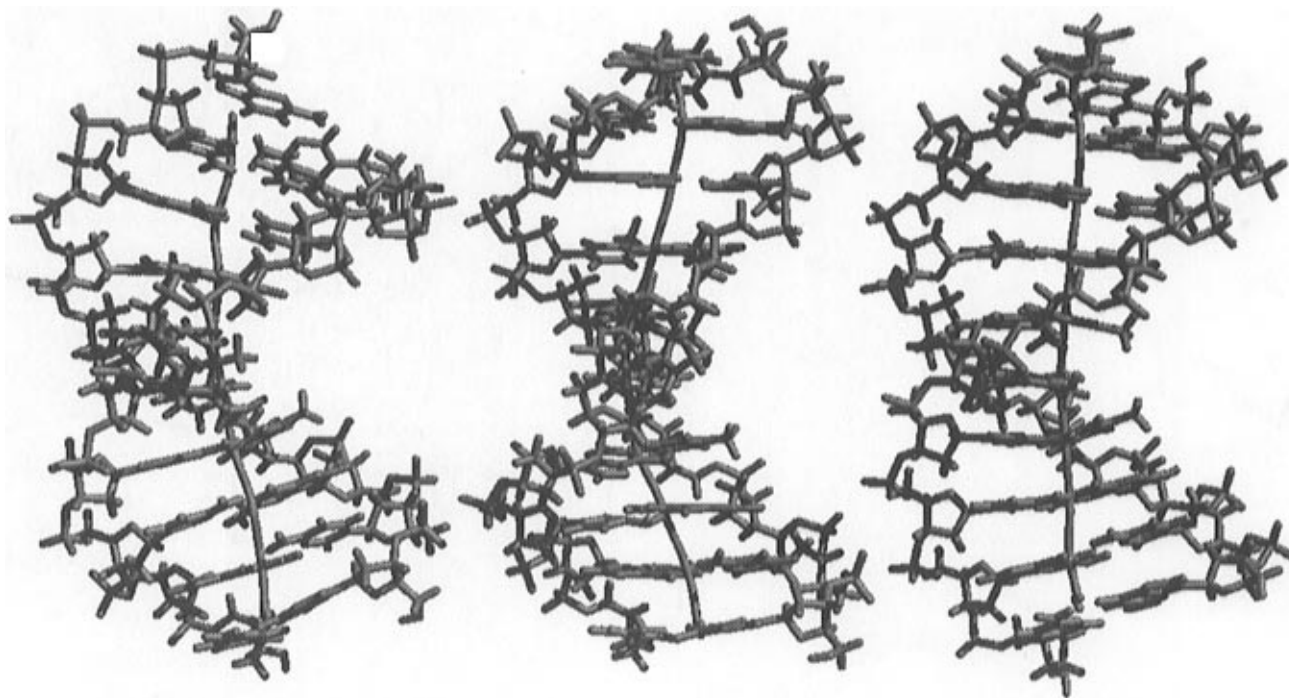


Figure 1. Average 580–800 ps structures of cis-syn thymine dimer (A, left), 6-4 pyridine–pyrimidone adduct (B, middle), and native duplex (C, right) of $d(\text{CGCATTACGC})_2$ with the axis of curvature generated from Curves.²⁰ The structures were best fit (RMSd) to line up with a common reference frame. All atoms are shown.

askiewicz *et al.* and, to our knowledge, the first unrestrained molecular dynamics study of a 6-4 adduct containing DNA duplex. Specifically we have performed 800 ps simulations of the photodamaged cis-syn dimer (A), 6-4 adduct (B), and undamaged B-DNA (C) duplex decamer $d(\text{CGCATTACGC})_2$ (Figure 1). The advantage of using this sequence is that both its cis-syn and 6-4 thymine dimer modified duplexes have been the subject of high-resolution NMR studies.⁵ Our computational study showed good agreement with the spectroscopically determined structures of the same DNA duplex⁵ and reveals the power of the PME method to accurately model not only canonical DNA forms but some unorthodox DNA structures as well.

Computational Methods

The creation of the initial structures, equilibration, and dynamics was performed as described previously.¹¹ The starting canonical B-form duplex geometries¹³ of the T-T cis-syn dimer of $d(\text{CGCATTACGC})_2$ (A), the T-T 6-4 adduct of $d(\text{CGCATTACGC})_2$ (B), and the control $d(\text{CGCATTACGC})_2$ (C) were generated with the NUCGEN module of AMBER 4.1.¹⁴ The force field parameters described by Cornell *et al.*¹⁵ [see also <http://www.amber.ucsf.edu>] were used in all of the simulations. For the cis-syn dimer and the 6-4 adduct modified atom types, charges (Figures 2 and 3) and modified force field parameters (Table 1) for the thymine residues were used. The modified charges for the lesion sites were generated with use of the RESP module of AMBER 4.1 for the isolated *N*-methyl derivatives of the T-T cis-syn dimer and 6-4 adduct shown in Figures 2 and 3. With use of these *N*-methylated model systems the lesion base charges were determined by imposing a charge of 0.126 (the charge on the DNA backbone at the lesion sites) on the methyl groups and performing a RESP charge optimization to yield a neutral model system. These RESP charges

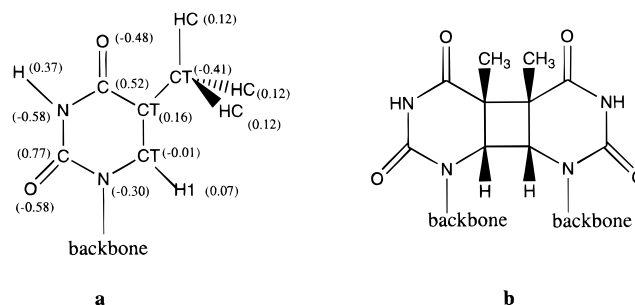


Figure 2. (a) Atom types and charges for T5 and T6 of cis-syn thymine dimer (A) and (b) isolated cis-syn dimer lesion.

were than assigned to the base atoms in the PREP module of AMBER 4.1 to yield new AMBER residues for use in the building of the photodamaged DNA duplexes in the LINK module of AMBER 4.1. Within LINK, cross-links between T5/CT5–T6/CT5 and T6/CT6–T6/CT6 of the cis-syn dimer and the T5(CT6)–T6(CM4) of the 6-4 adduct were also specified. Hydrogens were added with the EDIT module of AMBER 4.1, and the initial positions were minimized (in vacuo) to fix up poor hydrogen atom placement while holding all non-hydrogen atoms fixed. Explicit net-neutralizing sodium counterions were placed at the phosphates of these models by the EDIT module of AMBER 4.1 and the nucleic acid, and 18 counterions were surrounded by a periodic box of TIP3P waters which extended approximately 10 Å (in each direction) from the nucleic acid atoms. This leads to a periodic box size of $\sim 56 \text{ \AA} \times \sim 43 \text{ \AA} \times \sim 43 \text{ \AA}$ for each of the simulations. The simulations were performed with complete charges on the DNA with sodium counterions in a periodic box of TIP3P water molecules at atmospheric pressure and 298 K.

All simulations were run with the SANDER module of AMBER 4.1 with SHAKE¹⁶ (tolerance = 0.0005 Å) on the hydrogens, a 2 fs time step, a temperature of 300 K with Berendsen temperature coupling,¹⁷ a 9 Å cutoff applied to the Lennard-Jones interactions, and constant pressure with isotropic molecule based scaling.¹⁷ The non-bonded list was updated every 10 steps.

(16) Ryckaert, J. P.; Ciccotti, G.; Berendsen, H. J. C. *J. Comp. Phys.* **1977**, *23*, 327–341.

(17) Berendsen, H. J. C.; Postma, J. P. M.; van Gunsteren, W. F.; DiNola, A.; Haak, J. R. *J. Comp. Phys.* **1984**, *81*, 3684–3690.

(13) Arnott, S.; Hukins, D. W. *Biochem. Biophys. Res. Commun.* **1972**, *47*, 1504–1509.

(14) Pearlman, D. A.; Case, D. A.; Caldwell, J. W.; Ross, W. S.; Cheatham, T. E.; Debolt, S.; Ferguson, D.; Seibel, G.; Kollman, P. A. *Comput. Phys. Commun.* **1995**, *91*, 1–41.

(15) Cornell, W. D.; Cieplak, P.; Bayly, C. I.; Gould, I. R.; Merz, K. M.; Ferguson, D. M.; Spellmeyer, D. C.; Fox, T.; Caldwell, J. W.; Kollman, P. A. *J. Am. Chem. Soc.* **1995**, *117*, 5179–5197.

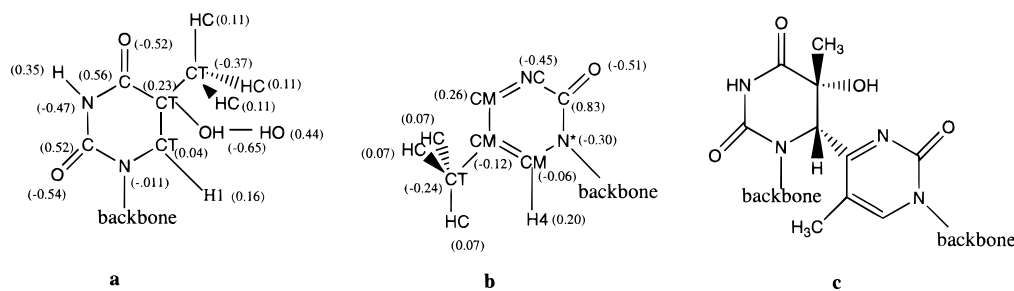


Figure 3. (a) Atom types and charges for T5 (pyrimidine) and (b) T6 (pyrimidone) of the 6-4 adduct (**B**) and (c) isolated 6-4 adduct lesion.

Table 1. Additional Force Field Parameters¹⁵

bond	K_r (kcal mol ⁻¹ Å ⁻²)	r_e (Å)
CM–NC	448.0	1.365
angle	K_θ (kcal mol ⁻¹ rad ⁻²)	θ_{eq} (deg)
CM–CM–CM	63.0	120.70
CM–CM–NC	70.0	121.20
CM–NC–C	70.0	120.50
N–CT–CM	50.0	109.50
H1–CT–CM	50.0	109.50
CT–CT–CM	50.0	109.50
CT–CM–NC	70.0	119.70
OS–CT–N	50.0	109.50
OS–CT–C	50.0	109.50
H2–CT–N	50.0	109.50
N–C–N	70.0	115.40
C–N–C	70.0	126.40
OH–CT–C	50.0	109.50

	idivf	$Vn/2$ (kcal mol ⁻¹)	γ (deg)	n
dihedral				
CM–CM–NC–C	4	7.40	180.00	2.0
CT–CM–NC–C	4	7.40	180.00	2.0
improper				
CM–CM–CM–CT		1.10	180.00	2.0

Equilibration was performed by first holding the positions of the DNA fixed and running 1000 steps of minimization followed by dynamics for 25 ps with a cutoff of 9 Å on all interactions. In order to avoid shifting of the two DNA strand molecules during constant pressure equilibration (when the DNA was held fixed), both strands were treated as if they were a single molecule. After this initial equilibration, all subsequent simulations were run by using the particle mesh Ewald method (PME)¹⁸ within AMBER 4.1 with a cubic B-spline interpolation order and a 10⁻⁵ tolerance for the direct space sum cutoff. To speed up the fast Fourier transform in the calculation of the reciprocal sum, the size of the PME charge grid is chosen to be a product of powers of 2, 3, and 5 and to be slightly larger than the size of the periodic box. This leads to a grid spacing of ~1 Å or less. Equilibration was continued with 25 kcal/(mol·Å) restraints placed on all solute atoms, minimization for 1000 steps, followed by 3 ps of MD, which allowed the water to relax around the solute. This equilibration was followed by 5 rounds of 600-step minimization where the solute restraints were reduced by 5 kcal/mol during each round. Finally, the system was heated from 100 to 300 K over 2 ps and then production runs were initiated.

All of the results were analyzed with the carnal module of AMBER 4.1, the Dials and Windows¹⁹ interface to Curves,²⁰ a more recent version of Curves, version 5.1 dated June 1996, or an adapted trajectory analysis software (RDPARM). Standard angle ($\alpha, \beta, \gamma, \delta, \epsilon, \zeta, \chi$)²¹ and helicoidal parameter²² names and definitions are presented in the

(18) Essmann, U.; Perera, L.; Berkowitz, M. L.; Darden, T.; Lee, H.; Pedersen, L. G. *J. Chem. Phys.* **1995**, *103*, 8577–8593.

(19) Ravishanker, G.; Swaminathan, S.; Beveridge, D. L.; Lavery, R.; Sklenar, H. *J. Biomol. Struct. Dyn.* **1989**, *6*, 669–99.

(20) Lavery, R.; Sklenar, H. *J. Biomol. Struct. Dyn.* **1988**, *6*, 63–91.

(21) Saenger, W. *Principles of Nucleic Acid Structure*; Springer-Verlag: New York, 1984.

(22) Dickerson, R. E. *Nucleic Acids Res.* **1989**, *17*, 1797–1803.

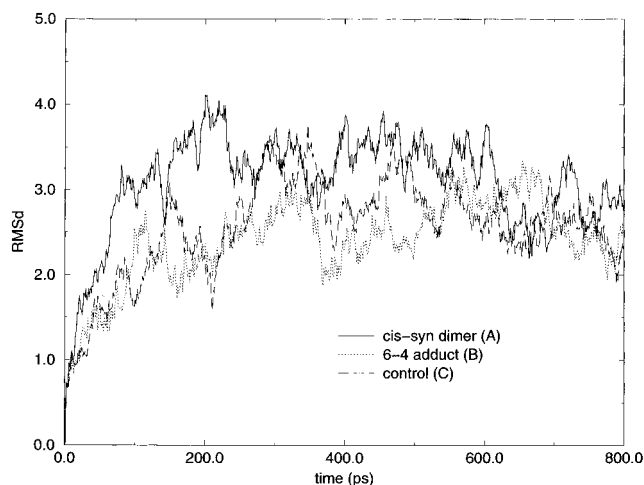


Figure 4. Comparison of the all atom RMSDs over 800 ps for the cis-syn thymine dimer (**A**), the 6-4 pyridine–pyrimidone adduct (**B**), and native duplex (**C**) of d(CGATTACGC)₂. Deviations are determined relative to the initial minimized and equilibrated structures.

analysis. Nucleic acid residue names are referred to in the text as one-letter codes with a residue number; the residue number is in the 5' to 3' direction with the first strand numbered 1–10 and the second strand 11–20. Average structures from the trajectories were calculated by using the carnal module of AMBER to coordinate average the RMS coordinate fit frames (over all DNA atoms) taken at 1 ps intervals. The helicoidal parameters were calculated from the 580–800 ps average structures.²³ All the molecular graphics images were produced by using the MidasPlus program from the Computer Graphics Laboratory, University of California, San Francisco. All simulations were run on 16 processors of the Cray T3D at the Pittsburgh Supercomputing Center. The Cray T3D parallel version was adapted from the MPI version of AMBER originally developed by Vincent and Merz²⁴ and incorporated into AMBER 4.1. Parallelization of the particle mesh Ewald code specifically for the Cray T3D and also more generally under MPI was performed by Michael Crowley of the Pittsburgh Supercomputing Center.

Results and Discussion

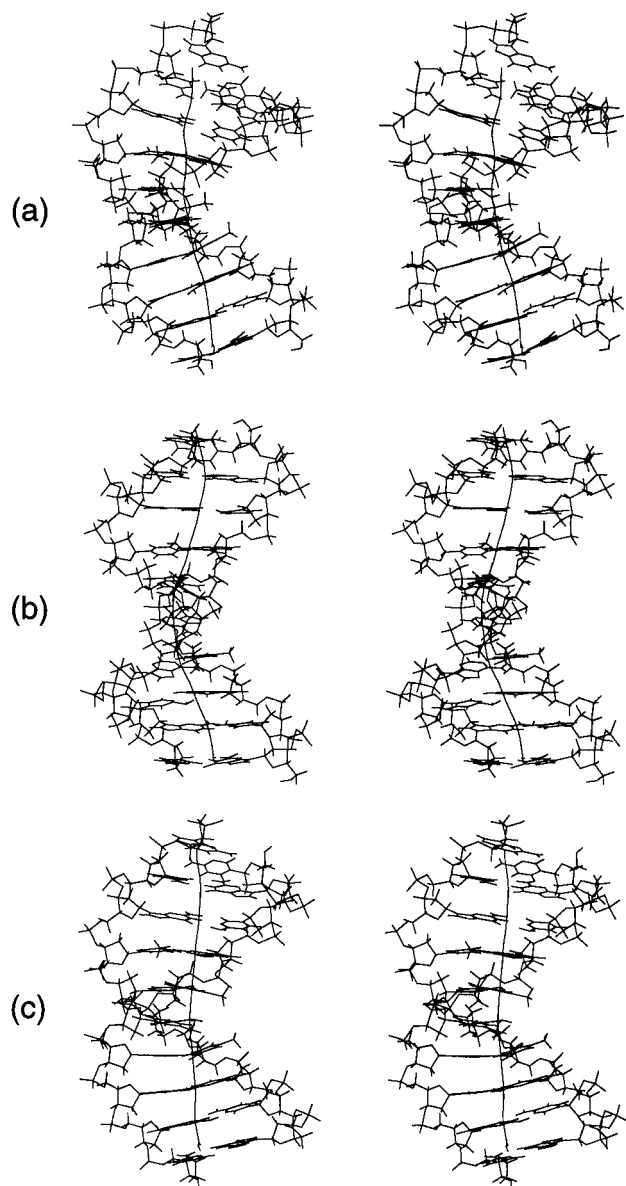
Simulated Structures. Starting from the canonical B forms of oligonucleotides **A**, **B**, and **C**, minimization, equilibration, and 800 ps unrestrained MD simulations were performed with use of the SANDER module of AMBER with PME code. In Figure 4, an all-atom RMSd plot for the complete MD simulation of structures **A**, **B**, and **C** is presented. To show whether our structures were converged at 800 ps the all-atom RMSDs between the average structures from 200–350, 350–580, and 580–800 ps for the cis-syn dimer, 6-4 adduct, and

(23) Analysis of the counterions and hydration of PME simulated DNA structures is discussed in the following: Cheatham, T. E.; Kollman, P. A. *Molecular Dynamics Simulations Highlight the Structural Differences Among DNA:DNA, RNA:RNA and DNA:RNA Hybrid Duplexes.* *J. Am. Chem. Soc.* submitted for publication.

(24) Vincent, J. J.; Merz, K. M. *J. Comp. Chem.* **1995**, *16*, 1420–1427.

Table 2. All Atom RMSDs (Å) between Minimized Average Structures

decamer	200–350 ps	350–580 ps	580–800 ps
cis-syn dimer (A)			
200–350 ps		0.74	1.20
350–580 ps	0.74		0.94
6-4 adduct (B)			
200–350 ps		0.84	0.92
350–580 ps	0.84		1.03
control (C)			
200–350 ps		0.99	0.81
350–580 ps	0.99		1.10

**Figure 5.** Stereoviews of the 580–800 ps average structures of the (a) cis-syn thymine dimer (A), (b) 6-4 pyridine-pyrimidone adduct (B), and (c) native duplex (C) of d(CGATTACGC)₂ with the axis of curvature generated from Curves.²⁰ The structures were best fit (RMSd) to line up with a common reference frame. All atoms are shown.

control were determined (Table 2). In total, considering subtle changes in the torsion and helicoidal structures, in addition to some fraying of the end base pairs over the course of a simulation, the small all-atom RMSDs indicate that our structures are reasonably converged.

In Figure 5, stereoviews of structures A, B, and C are presented. In each case the structures were minimized with a

Table 3. Backbone Torsion Values (deg) for Cis-Syn Dimer A, 6-4 Adduct B, and control C^a

	α	β	γ	δ	ϵ	ζ	χ
(a) Cis-Syn Dimer A							
C1	279.6	75.7 ^a	50.1	117.2	214.1 ^b	252.1 ^b	235.1
G2	291.7	167.1	56.9	132.1	185.5	267.6	249.7
C3	292.2	174.4	58.3	101.7	186.1	271.4	229.9
A4	292.7	184.3	47.7	128.5	186.8	268.7	244.4
T5	292.0	156.6	50.7	128.0	180.7	276.0	297.3
T6	293.4	174.3	54.0	93.8	206.2	239.1	221.9
A7	285.3	169.4	51.2	133.7	194.8	275.1	237.5
C8	277.1	153.2	46.1	132.9	264.5 ^b	172.7 ^b	261.5
G9	282.7	159.9	52.1	135.4	214.4	254.4	245.9
C10				121.4			258.0
G20	291.6	171.6	54.6	114.4	188.7	275.6	236.0
C19	290.2	164.7	56.4	103.64	192.3 ^b	254.6 ^b	228.9
G18	289.9	172.3	51.8	118.7	189.8	272.8	245.3
T17	292.9	171.5	56.6	112.8	189.2	273.9	238.7
A16	289.5	173.8	53.9	109.9	187.0	263.2	227.4
A15	289.5	173.2	54.9	118.2	187.2	270.9	241.7
T14	293.6	169.2	60.1	116.3	185.7	270.3	238.8
G13	290.0	169.1	55.5	114.2	190.4	258.3	238.0
C12	272.0	144.6	56.6	133.7	278.0 ^b	122.9 ^b	247.3
G11				137.2			294.0
(b) 6-4 Adduct B							
C1	251.4	167.8	60.8	142.1	277.9	79.9 ^b	41.9 ^b
G2	292.3	165.5	57.9	146.3	180.4	268.9	263.4
C3	290.6	164.0	55.1	107.0	206.5	244.2	234.6
A4	301.8	167.9	66.0	120.5	184.5	271.2	232.8
T5	279.8	174.2	50.8	79.9	241.1	294.2	216.8
T6	240.8	163.6	71.9	142.9	281.9	105.9	308.7
A7	291.9	166.9	52.6	142.1	187.5	274.4	252.0
C8	286.1	167.6	49.6	122.1	219.6	223.1	248.9
G9	287.0	170.6	52.3	29.7 ^b	191.6	273.9	236.1
C10				115.6			244.5
G20	291.4	169.88	52.8	119.2	188.6	272.9	240.9
C19	282.9	139.9	50.8	135.3	277.01	143.03	239.5
G18	283.9	173.1	46.4	138.6	196.8	281.5	263.8
T17	295.5	169.9	57.2	109.6	182.1	267.8	231.3
A16	270.9	141.5	61.3	139.6	279.8 ^b	119.7 ^b	254.9
A15	268.0	164.8	40.6	127.5	219.6	289.8	297.6
T14	293.3	174.4	55.9	109.4	185.7	267.9	227.7
G13	294.4	169.8	57.8	116.4	185.8	265.9	229.6
C12	279.8	151.3	56.7	129.7	249.2 ^b	175.2 ^b	243.2
G11				129.4			267.6
(c) Control C							
C1	278.2	163.5	49.3	133.3	250.9	175.7	268.6
G2	293.1	167.4	56.4	140.0	186.1	270.7	245.4
C3	291.2	168.7	57.0	107.8	188.6	269.5	236.6
A4	299.5	168.3	61.4	111.0	180.1	267.7	237.8
T5	293.9	171.8	55.5	115.3	186.1	269.4	232.5
T6	291.9	170.6	51.9	121.2	188.1	272.1	240.8
A7	289.7	172.2	54.8	104.8	189.1	272.2	229.1
C8	289.8	167.4	55.9	109.8	197.2	250.9	235.1
G9	290.6	167.5	55.1	122.2	189.0	271.4	241.5
C10				103.6			229.8
G20	289.8	168.9	54.8	121.3	191.2	272.4	246.9
C19	283.7	137.8	47.7	125.3	275.2	151.7	235.8
G18	285.0	173.9	42.9	137.3	192.8	279.0	264.8
T17	294.9	172.9	55.9	113.6	186.3	270.5	234.1
A16	295.9	169.0	59.1	112.1	184.3	267.4	226.6
A15	291.6	172.6	56.6	114.7	186.7	275.2	233.9
T14	292.1	166.4	58.9	99.7	185.1	268.5	228.7
G13	284.7	159.2	49.1	135.5	230.8	205.3	249.9
C12	279.4	172.5	49.2	129.2	204.4	278.0	258.1
G11				119.3			212.6

^a T5/T6 torsion values in boldface. ^b Non-lesion torsions which vary significantly from control C values.

constant dielectric until the RMSd in energy between steps changed by less than 0.1 kcal/mol to correct the overlap of hydrogens which result from rotation of the methyl groups over the course of the simulation. Considering the large distortions associated with the introduction of the cis-syn and 6-4 lesion

Table 4. Helicoidal Values (deg) for **A**, **B**, and **C**^a

	buckle	prop	open	tilt	roll	twist
A						
C1/G20	5.3	-17.9	2.2			
G2/C19	1.8	-11.2 ^b	0.6	-7.9	8.5	34.9
C3/G18	-0.6	-11.4	0.7	-2.6	0.2	31.3
A4/T17	2.9	-16.8	3.3	-2.1	11.8	31.7
T5/A16	36.0	-47.4	9.2	11.0	-10.3	32.5
T6/A15	-5.4	-2.1	6.1	-11.7	36.3	23.8
A7/T14	-4.9	-10.4 ^b	6.6	0.2	5.9 ^b	33.3
C8/G13	8.7	-7.9	1.5	5.9	5.6	26.5
G9/C12	-3.5	-18.4 ^b	-1.4	1.3	-4.6	38.5
C10/G11	1.5	5.9	1.7	6.9	-8.0	34.2
B						
C1/G20	60.8 ^b	-31.9 ^b	15.4 ^b			
G2/C19	-0.3	-28.8	1.1	-12.1	16.3	36.7
C3/G18	-10.3	2.9	1.7	6.2	-8.4	34.7
A4/T17	-4.5	-11.5	1.2	1.2	20.2	27.6
T5/A16	-12.9	-38.2	2.8	6.3	-10.5	30.5
T6/A15	11.2	30.5	-37.9	12.8	25.1	25.9
A7/T14	22.8 ^b	-22.0	-0.2	-13.4 ^b	0.0 ^b	17.1 ^b
C8/G13	17.6 ^b	-20.4 ^b	3.1	0.0	7.2	29.3
G9/C12	-8.6	-18.2 ^b	-0.4	-2.4	13.0	35.3
C10/G11	-4.1	3.2	2.1	3.9	3.9	34.2
C						
C1/G20	13.1	-11.2	1.9			
G2/C19	0.1	-20.9	-2.0	-8.5	1.9	37.5
C3/G18	-6.5	-4.6	1.4	1.3	-9.1	35.7
A4/T17	4.4	-13.4	4.2	-2.8	17.3	26.3
T5/A16	7.5	-16.5	2.2	-0.9	0.8	30.2
T6/A15	4.3	-19.2	3.8	1.7	4.9	31.8
A7/T14	-5.9	-20.6	8.8	-2.7	15.6	29.3
C8/G13	-6.9	-8.9	0.9	4.9	6.6	28.7
G9/C12	-3.5	-3.1	-0.0	7.5	3.9	36.2
C10/G11	7.1	-3.9	-0.2	1.1	4.8	30.3

^a T5/T6 (lesion) helicoidal values in bold face. ^b Non-lesion helicoidal values which vary significantly from control **C** values.

into the canonical B-forms of the decamer it is noteworthy that the structures maintain their duplex integrity and, as found by Cheatham and Kollman¹¹ and by NMR,⁵ are clearly B-DNA like.

In Tables 3a, 3b, 3c, and 4 and Figures 6 and 7, pertinent backbone and base parameters for the 580–800 ps simulated structures are presented. For both photodamaged decamers the greatest differences in the torsional and helicoidal parameters relative to the control occur primarily at the lesion sites. The most notable distortions in torsion angles of the cis-syn dimer (**A**) are the A-DNA-like δ at T6 and syn χ at T5. Miaskiewicz *et al.* reports these same torsional distortions for his simulated cis-syn containing dodecamer.¹² In addition, a syn χ angle at the 5'T was reported by Alderfer *et al.* for his dimer containing polyA–polyT hexamer and dodecamer,¹⁰ and experimentally from the crystal structure of the isolated T-T dimer.²⁵ The cis-syn dimer also has a large positive buckle and tilt, and negative propeller and roll, at the first TA base step, and substantial negative tilt and positive roll at the second TA step relative to the control (**C**). These same distortions in the helicoidal base parameters were reported by Miaskiewicz *et al.* for their simulated cis-syn containing dodecamer.¹² Other significant deformations in the cis-syn containing decamer are the increased ϵ and ζ values at the G11 and C8 and the large positive χ at G11.

Not surprisingly, the 6-4 lesion creates a larger disturbance in the structure of the decamer than the cis-syn dimer. Most notably, there are substantial deviations in the sugar and backbone parameters α , ϵ , ζ , and χ at the lesion site. More significant, however, are the observed changes in the base

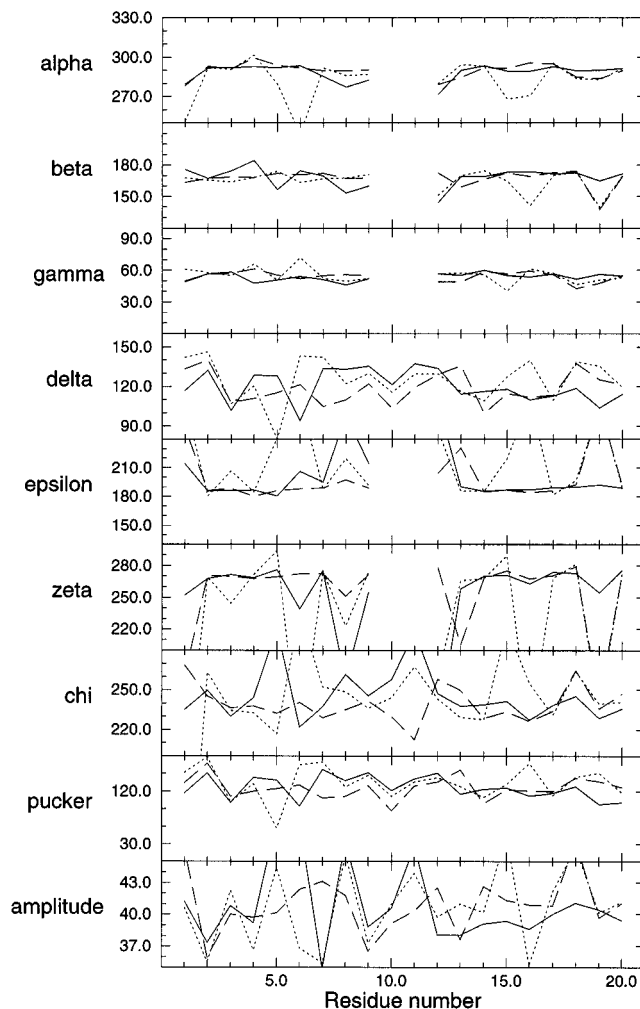


Figure 6. Backbone torsion values (deg) of the 580–800 ps structures of the cis-syn thymine dimer (**A**) (—), the 6-4 pyridine–pyrimidone adduct (**B**) (···), the native duplex (**C**) (---) of d(CGATTACGC)₂. All of the values were calculated with Dials and Windows.¹⁹

parameters relative to the control. Thus, at the T5-A16 base pair there is a large negative propeller and at the T6-A15 step there is a large positive tilt, propeller, and roll. Significant negative tilt and twist at the A7-T14 base pair flanking the lesion to the 3' side is also apparent. These base pair parameters reflect Kim *et al.*'s experimentally observed break in the standard sequential NOEs to the 3' side of the 6-4 lesion.⁵ For the 6-4 adduct there is a large opening between the oxidized base T6 and A15, and a moderate opening is also found for the T5-A16 base pair of the cis-syn dimer. These openings are consistent with the "hole" at the photodimer site reported by Vassilyev for the crystal structure of the DNA duplex–T4 endonuclease V complex.⁶ The average 580–800 ps structure of the 6-4 adduct (**B**) also has large deviations in the backbone and base parameters at the C1-G20 step, indicative of end base pair fraying. Specifically, the χ angle at C1 flipped from anti to syn, resulting in very large deviations in the C1-G20 buckle and propeller and a large opening between the C1 and G20 bases. In addition, the C1:H41–G20:O6 (2.97 ± 0.68 Å) and C1:N3–G20:H1 (2.26 ± 0.30 Å) hydrogen bonds of **B** are significantly longer than the same hydrogen bonds of the control (2.05 ± 0.19 and 2.02 ± 0.11 Å, respectively).

Effects on the complementary strands of **A** relative to the control (**C**) indicate that the conformational rigidity of the dimer leads to a decrease in the variability of the backbone torsions in the complementary strand. Excluding the C10-G11 end base

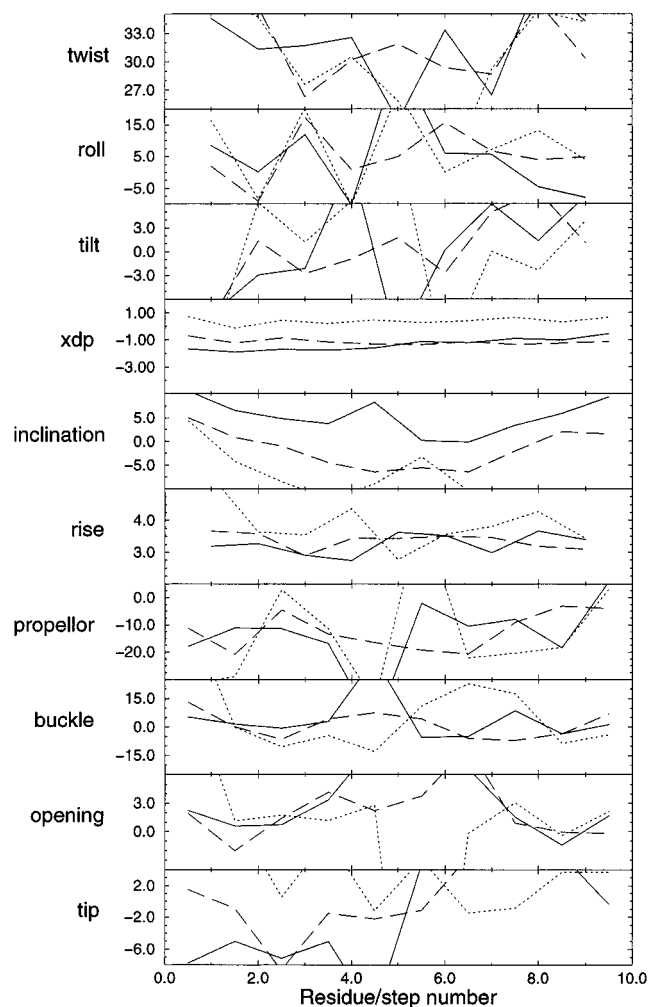


Figure 7. Helicoidal base values (deg) of the 580–800 ps structures of the cis-syn thymine dimer (A) (—), the 6-4 pyridine–pyrimidine adduct (B) (···), and the native duplex (C) (---) of d(CGATTACGC)₂. All of the values were calculated with Dials and Windows.¹⁹

Table 5. Calculated and Experimental Backbone Torsion Values (deg) of T5 and T6 of the 6-4 Adduct Containing Decamer

	α	β	γ	δ	ϵ	ζ	χ
calcd							
T5	279.8	174.2	50.84	79.9	241.1	294.2	216.8
T6	240.8	163.6	71.9	142.9	281.9	105.9	308.7
exptl ⁵							
T5				89	246		211
T6	148	214	56	105		278	299

pair, this is most noticeable in the ϵ and ζ torsions of the phosphate backbone. These backbone torsions indicate that the conformationally constrained T5-T6 dimer leads to a slight locking down of the motions of the decamer. The conformational constraints of the T5-T6 dimer are also reflected in the cis-syn containing decamers A-DNA-like base inclination. These same constraints are not found for the complementary strand of the 6-4 adduct. In fact, contrary to the relative rigidity in the complementary strand of the dimer (A), the variability of the ϵ , ζ , and χ angles of the A15 and A16 base pairs opposite the 6-4 lesion implies an increase in the flexibility of the complementary backbone relative to the control. Presumably this added flexibility is facilitated by the break in the Watson–Crick hydrogen bonding between T6 and A15.

Comparison with Experiment. A comparison of the torsion angles suggested from the NMR refined structure⁵ of the 6-4

Table 6. Experimental NOEs and Calculated Interproton Distances (Å) for Cis-Syn Dimer (A) and Control (C) and 6-4 Adduct (B) and Control (C)

NOE (exp.) ⁵	interproton distances (calc)	
	580–800 ps ^a	control (C) ^a
(a) Cis-Syn Dimer (A)		
T5(H6)/T6(CH ₃) strong	2.58 (0.20)	3.92 (0.79)
T6(H6)/T5(CH ₃) medium	4.41 (0.16)	6.54 (0.50)
standard sequential NOE		
interstrand		
C1(NH ₂)/G20(NH)	2.46 (0.31)	2.45 (0.29)
G2(NH)/C19(NH ₂)	2.49 (0.25)	2.50 (0.26)
C3(NH ₂)/G18(NH)	2.42 (0.26)	2.41 (0.27)
A4(H2)/T17(NH)	2.88 (0.24)	2.82 (0.22)
T5(NH)/A16(H2) strong	3.00 (0.29)	2.83 (0.24)
T6(NH)/A15(H2) strong	2.93 (0.26)	2.85 (0.25)
A7(H2)/T14(NH)	2.81 (0.23)	2.82 (0.26)
C8(NH ₂)/C13(NH)	2.42 (0.27)	2.45 (0.27)
C9(NH)/C12(NH ₂)	2.38 (0.25)	2.45 (0.23)
A4(H2)/G18(NH)	4.45 (0.58)	4.44 (0.41)
T6(NH)/A16(H2)	4.41 (0.49)	3.59 (0.43)
A4(NH ₂)/T17(NH)	2.45 (0.25)	2.40 (0.25)
A7(H2)/G13(NH)	4.01 (0.52)	4.11 (0.45)
intrastrand		
lesion strand		
A4(H2)/T5(NH)	3.45 (0.38)	3.98 (0.43)
T6(NH)/A7(H2)	5.58 (0.43)	5.36 (0.44)
complementary strand		
T14(NH)/A15(H2)	4.80 (0.51)	5.30 (0.43)
A16(H2)/T17(NH)	4.06 (0.47)	4.02 (0.42)
(b) 6-4 Adduct (B)		
T5(CH ₃)/T6(CH ₃) medium	5.32 (0.75)	4.47 (1.05)
T5(H6)/T6(CH ₃) strong	2.75 (0.58)	3.92 (0.79)
T5(CH ₃)/A4(H1')	5.37 (0.34)	5.48 (0.70)
T5(CH ₃)/A4(H2')	4.45 (0.68)	3.73 (0.81)
T5(CH ₃)/A4(H2'')	4.71 (0.74)	4.17 (0.83)
T5(CH ₃)/A4(H3')	6.55 (0.83)	5.69 (0.90)
T5(CH ₃)/A4(H4')	7.69 (0.72)	7.27 (0.83)
A4(H1')/A4(H2)	4.55 (0.14)	4.50 (0.14)
A7(H1')/A7(H2)	4.52 (0.14)	4.51 (0.15)
A16(H1')/A16(H2)	4.53 (0.14)	4.53 (0.14)
A4(H1')/T6(CH ₃)	5.98 (1.03) ^b	7.74 (0.91)
A4(H2)/T5(H1')	3.23 (0.48)	4.16 (0.57)
A7(H2)/C8(H1')	4.70 (0.76)	4.49 (0.79)
A16(H2)/T17(H1')	4.24 (0.59)	3.98 (0.54)
standard sequential NOE		
interstrand		
C1(NH ₂)/G20(NH)	3.35 (0.60)	2.45 (0.29)
G2(NH)/C19(NH ₂)	2.48 (0.25)	2.50 (0.26)
C3(NH ₂)/G18(NH)	2.39 (0.25)	2.41 (0.27)
A4(H2)/T17(NH)	2.80 (0.26)	2.82 (0.22)
T5(NH)/A16(H2) weak	3.00 (0.29)	2.83 (0.24)
A7(H2)/T14(NH)	2.85 (0.22)	2.82 (0.26)
C8(NH ₂)/C13(NH)	2.44 (0.25)	2.45 (0.27)
C9(NH)/C12(NH ₂)	2.44 (0.23)	2.45 (0.23)
C10(NH ₂)/G11(NH)	2.48 (0.29)	2.58 (0.31)
G2(NH)/G18(NH)	3.64 (0.32)	3.39 (0.32)
A4(H2)/A16(H2)	5.43 (0.57)	4.84 (0.44)
A4(H2)/G18(NH)	4.66 (0.45)	4.44 (0.41)
A7(H2)/G13(NH)	4.88 (0.42)	4.11 (0.45)
A7(H2)/A15(H2)	3.68 (0.58)	4.01 (0.39)
G9(NH)/G13(NH)	4.37 (0.43)	3.72 (0.35)
intrastrand		
lesion strand		
T5(NH)/A4(H2) weak	4.75 (0.53)	4.00 (0.44)
complementary strand		
G12(NH ₂)/G13(NH)	4.25 (0.61)	4.29 (0.58)
A16(H2)/T17(NH) weak	4.57 (0.58)	4.02 (0.42)
T17(NH)/G18(NH)	4.40 (0.38)	4.24 (0.35)

^a Standard deviations in parentheses. ^b A4(H1')/T6(CH₃) from 800–1150 ps = 5.91 ± 0.24 Å.

lesion (Table 5) with our simulated values finds considerable coincidence in the sugar and backbone torsions β , δ , ϵ , and χ . The backbone torsions, α and ζ , which are further from the

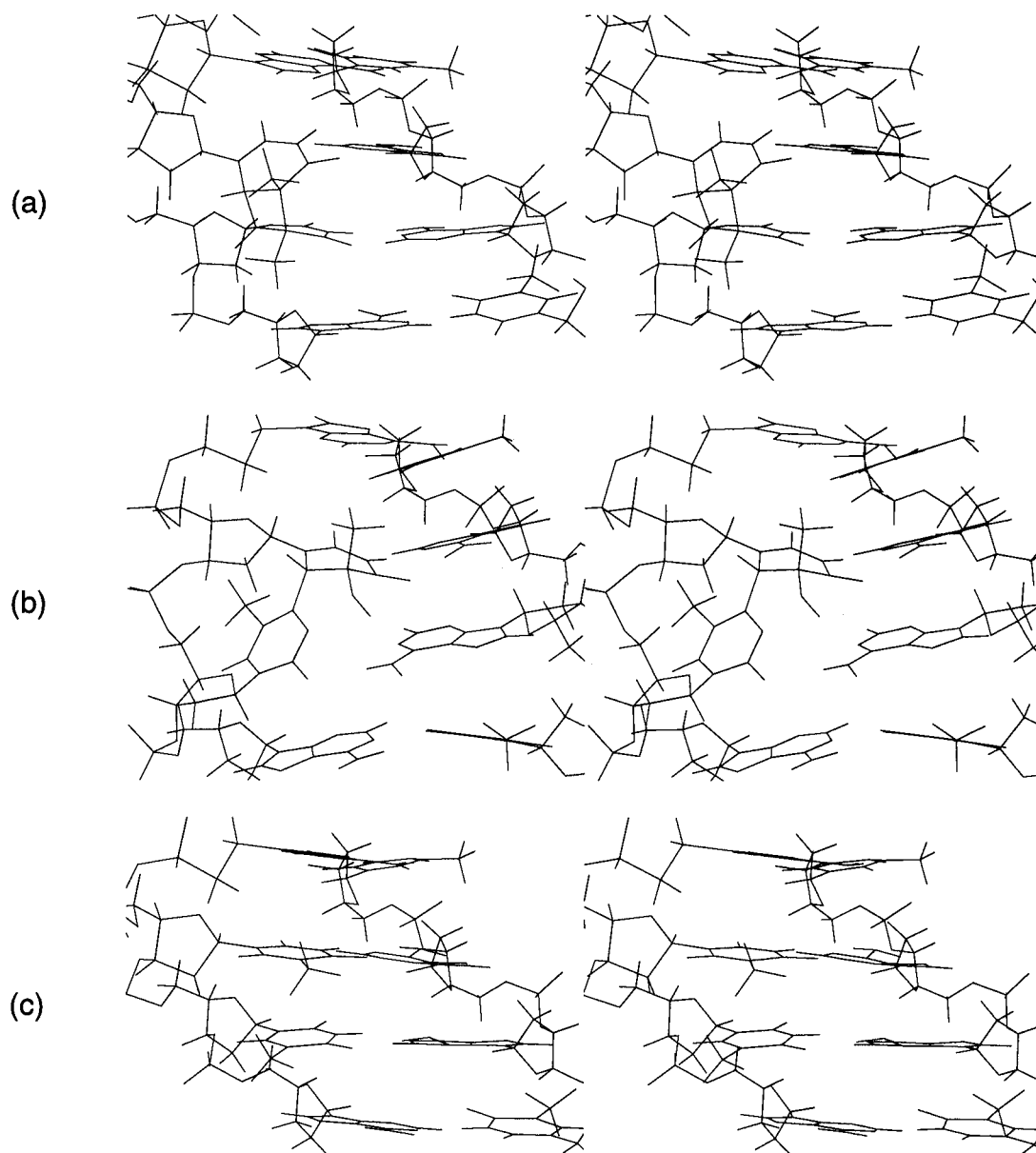


Figure 8. Stereoviews of the d(ATTA)₂ region of the (a) cis-syn thymine dimer (**A**), (b) the 6-4 pyridine-pyrimidone adduct (**B**), and (c) the native duplex (**C**) of d(CGCAATTACGC)₂. The structures were best fit (RMSd) to line up with a common reference frame. All atoms are shown.

lesion site, are not the same as in the NMR structure. Specifically, while we observe an α of g^- and a ζ of g^+ , Kim *et al.* reports a g^+ torsion for α and a g^- torsion for ζ . Unfortunately, because it is not possible to experimentally determine the difference between these torsion angles without applying phosphorus NMR, we cannot determine the significance of this difference between the simulated and experimentally derived structures. Nevertheless, because Kim *et al.*'s structural refinement protocol involved initial model building of the duplex from the crystal structure of the isolated dithymidine cis-syn dimer and 6-4 adduct,⁵ while our lesions were created by modification of the thymine residues of the decamer in AMBER 4.1, the differences between the calculated and experimental torsions at the lesion sites are not surprising. Kim *et al.* also reports a 44° angle for the T5N(1)–C(6)–T6C(4)–N(3) dihedral,⁵ which compares well to the 55° dihedral of our simulated structure. Although not reported by Kim *et al.*, this same dihedral angle for the simulated cis-syn dimer (**A**) and control (**C**) is 18° and 38° , respectively. As found in the experimentally derived structures, our calculated dihedrals indicate that the T5 and T6 bases of the 6-4 adduct are

perpendicular to one another, while those of the cis-syn dimer are stacked in parallel.⁵

In Table 6 the experimental NOEs⁵ and our interproton distances for the simulated structures **A**, **B**, and **C** are presented. We assume that any distance whose value (including standard deviations) is $<5 \text{ \AA}$ should be observed. Kim *et al.*⁵ and Taylor⁴ report that when the cis-syn dimer is embedded in a DNA duplex the conformational flexibility of the cyclobutane ring observed for the isolated T-T dimer is lost.²⁶ Specifically, Kim *et al.* observed a stronger intensity NOE for the T5(H6)–T6(CH₃) than for the T6(H6)–T5(CH₃) NOE, indicating a CB+ conformation for the cyclobutane ring.⁵ Our interproton data for the analogous protons also suggest a CB+ conformation. This CB+ conformation is also clearly evident in Figure 8.

Experimentally, the observed T5(NH)–A16(H2) and T6(NH)–A15(H2) NOEs indicate standard Watson–Crick bonding at the cis-syn lesion.⁵ Again, our interproton distances (Table 6a) and Figure 8 show that the hydrogen bonding is also intact in the simulated structure. Examination of Table 7 and Figure

(26) Alderfer, J. L.; Kim, J.-K. *J. Biomol. Struct. Dyn.* **1992**, *9*, 705–718.

Table 7. Hydrogen Bond Lengths (Å) of Six Central Base Pairs of **A**, **B**, and **C**^a

decamer	hydrogen bond		length (Å)	
cis-syn dimer (A)	C3:H41	G18:O6	2.03 (0.18)	
	C3:N3	G18:H1	2.02 (0.10)	
	C3:O2	G18:H21	1.93 (0.13)	
	A4:H61	T17:O4	2.08 (0.27)	
	A4:N1	T17:H3	2.04 (0.14)	
	T5:H3	A16:N1	2.33 (0.23)	
	T5:O4	A16:H61	2.07 (0.20)	
	T6:H3	A15:N1	2.08 (0.16)	
	T6:O4	A15:H61	2.04 (0.19)	
	A7:H61	T14:O4	2.01 (0.13)	
	A7:N1	T14:H3	2.16 (0.33)	
	C8:H41	G13:O6	1.91 (0.12)	
	C8:N3	G13:H1	2.03 (0.10)	
	C8:O2	G13:H21	2.04 (0.17)	
	6-4 adduct (B)	C3:H41	G18:O6	1.96 (0.15)
		C3:N3	G18:H1	1.97 (0.10)
		C3:O2	G18:H21	1.91 (0.12)
		A4:H61	T17:O4	2.00 (0.16)
		A4:N1	T17:H3	2.03 (0.14)
		T5:H3	A16:N1	2.00 (0.12)
T5:O4		A16:H61	2.10 (0.30)	
T6:O2		A15:H61	2.99 (0.53)^b	
A7:H61		T14:O4	2.05 (0.16)	
A7:N1		T14:H3	1.98 (0.17)	
C8:H41		G13:O6	1.86 (0.11)	
C8:N3		G13:H1	1.96 (0.10)	
C8:O2		G13:H21	2.02 (0.19)	
control (C)		C3:H41	G18:O6	2.02 (0.17)
		C3:N3	G18:H1	2.01 (0.10)
		C3:O2	G18:H21	1.92 (0.14)
		A4:H61	T17:O4	2.08 (0.20)
		A4:N1	T17:H3	2.01 (0.11)
		T5:H3	A16:N1	2.03 (0.13)
		T5:O4	A16:H61	2.05 (0.17)
	T6:H3	A15:N1	2.05 (0.16)	
	T6:O4	A15:H61	2.09 (0.25)	
	A7:H61	T14:O4	2.01 (0.13)	
	A7:N1	T14:H3	2.40 (0.45)	
	C8:H41	G13:O6	1.93 (0.12)	
	C8:N3	G13:H1	2.02 (0.10)	
	C8:O2	G13:H21	2.10 (0.21)	

^a Standard deviations in parentheses. T5/T6 (lesion) base pairs in boldface. ^b Determined from 800–1150 ps trajectory.

9, which present the hydrogen bond distance between the lesion base pairs for **A**, **B**, and **C**, shows that there is a slight lengthening of the T5(H3)–A16(N1) hydrogen bond. Miaskiewicz *et al.*'s dodecamer simulation also yielded a lengthening of this same hydrogen bond.¹² It is worthy of note that, consistent with our simulation results and those of Miaskiewicz *et al.*,¹² the X-ray structure of the T4 endonuclease/cis-syn dimer duplex complex⁶ finds the 5'T adenine–thymine hydrogen bond broken, suggesting that this hydrogen bond is weaker than that of the 3'T of the cis-syn dimer.

For the 6-4 adduct, Kim *et al.* reports a medium T5(CH₃)–T6(CH₃) NOE, and strong T5(H6)–T6(CH₃) NOE, reflecting the *R* stereochemistry of the linkage between the adjacent thymines.⁵ As shown in Table 6b, these relative NOEs and the associated *R* stereochemistry are also well represented by our simulated interproton distances. In addition, our T5(CH₃)–A4(H1', H2', and H2'') and A4(H2), A7(H2), and A16 (H2) distances with the H1' protons of their own and their 3' flanking residue are reflected by the experimentally observed NOEs.

Of particular interest is the unusual A4(H1')–T6(CH₃) NOE observed experimentally.⁵ This NOE was also reflected in the interproton distance of 5.91 ± 0.24 Å determined for these same protons in the simulated structure **B** (Table 6b). In fact, analysis of the simulated structure finds the T6 methyl significantly closer

to the A4 deoxyribose (Figure 8) than it is in Kim *et al.*'s refined NMR structure (a view of Figure 6 in ref 5 suggests a considerably larger distance for A4(H1')–T6(CH₃) than found here).⁵ Thus, the simulated structure better accounts for the experimental observation of this unusual NOE. Although Kim *et al.* notes that NOEs are observed between T5(CH₃) and all of the sugar protons of A4, based on the distances in Table 6b, only H1', H2', and H2'' should be close enough to observe NOEs. However, Kim *et al.*'s structure (Figure 6 in ref 5) also has H3' and H4' of A4 far from T5(CH₃), so it is likely that these NOEs may be due to spin diffusion. On further inspection it is also apparent that the relatively close proximity of the T6 methyl to the A4 sugar in the simulated structure is a result of the geometric constraints imposed by hydrogen bonding between the carbonyl of the T6 pyrimidone and the A15 NH₂. Specifically, analysis of the 6-4 dimer's 580–800 ps trajectory yielded a reasonable average T6:O2–A15:H61 hydrogen bond distance of 2.64 ± 0.46 Å. However, because our data also showed that this hydrogen bond was increasing in length over the course of the 580–800 ps trajectory, we continued the simulation of the 6-4 dimer (**B**) for 350 ps. As shown in Figure 9, this 800–1150 ps simulation yielded a T6:O2–A15:H61 hydrogen bond distance that is decreasing slightly over the course of the trajectory with an average hydrogen bond length of 2.99 ± 0.53 Å (Table 7). This hydrogen bond, which persists throughout the simulation trajectory, is notably longer than the standard 2.0 Å hydrogen bond length, and therefore it is probably more accurate to describe the interaction between the T6:O2 and A15:H61 as a long hydrogen bond or as a significant dipole–dipole interaction. Nevertheless, what is most significant is that this same hydrogen bond/dipole–dipole interaction is not found in the NMR-derived structure.

In keeping with studies on the relative repair rates of the cis-syn dimer and 6-4 adduct, which postulate that the larger deformation in a 6-4 adduct containing DNA duplex lead to greater recognition by repair enzymes,²⁷ we find that the 6-4 decamer deviates most, and the control deviates least, from canonical B-DNA helicity. Excluding the end base pairs, the largest deviation from helicity of the 6-4 adduct occurs at the fifth base steps. For the cis-syn dimer, the largest deviations are also found at the fifth base pair. Thus, as also reported by Miaskiewicz *et al.* there is a bend of approximately 15° at the T5/T6 base pair of the dimer lesion relative to the control.¹² Notably, the total angle of curvature between the first and last helical axis segments (i.e., the overall helical bend into the major groove) of the averaged simulated structures **A**, **B**, and **C** are 22.3°, 13.6°, and 8.2°, respectively. Clearly, our overall bending angle of 5° relative to the control for the 6-4 adduct disagrees with the 44° value of the NMR-determined structure. Part of this disagreement between the simulated and experimental structure could be a result of differences in model building strategy. Specifically, as noted earlier, the NMR refinement protocol yielded a structure with α and ζ torsions at T6 of g+ and g–, respectively,⁵ while these same torsions for the simulated structure were g– (α) and g+ (ζ). We postulate that this reversal of the torsion angles at the lesion site might account for the conflicting overall bending angles of the NMR-determined and simulated 6-4 adducts.

We also note that the NMR structure was refined by using a distance-dependent dielectric constant in vacuo, using the NMR restraints at high temperature, with room temperature dynamics carried out for only 20 ps. This short time and/or the simplicity of the solvation model used compared to that used here may

(27) Taylor, J.-S.; Svoboda, D. L.; Smith, C. A.; Sancar, A. *J. Biol. Chem.* **1993**, *268*, 10694–10700.

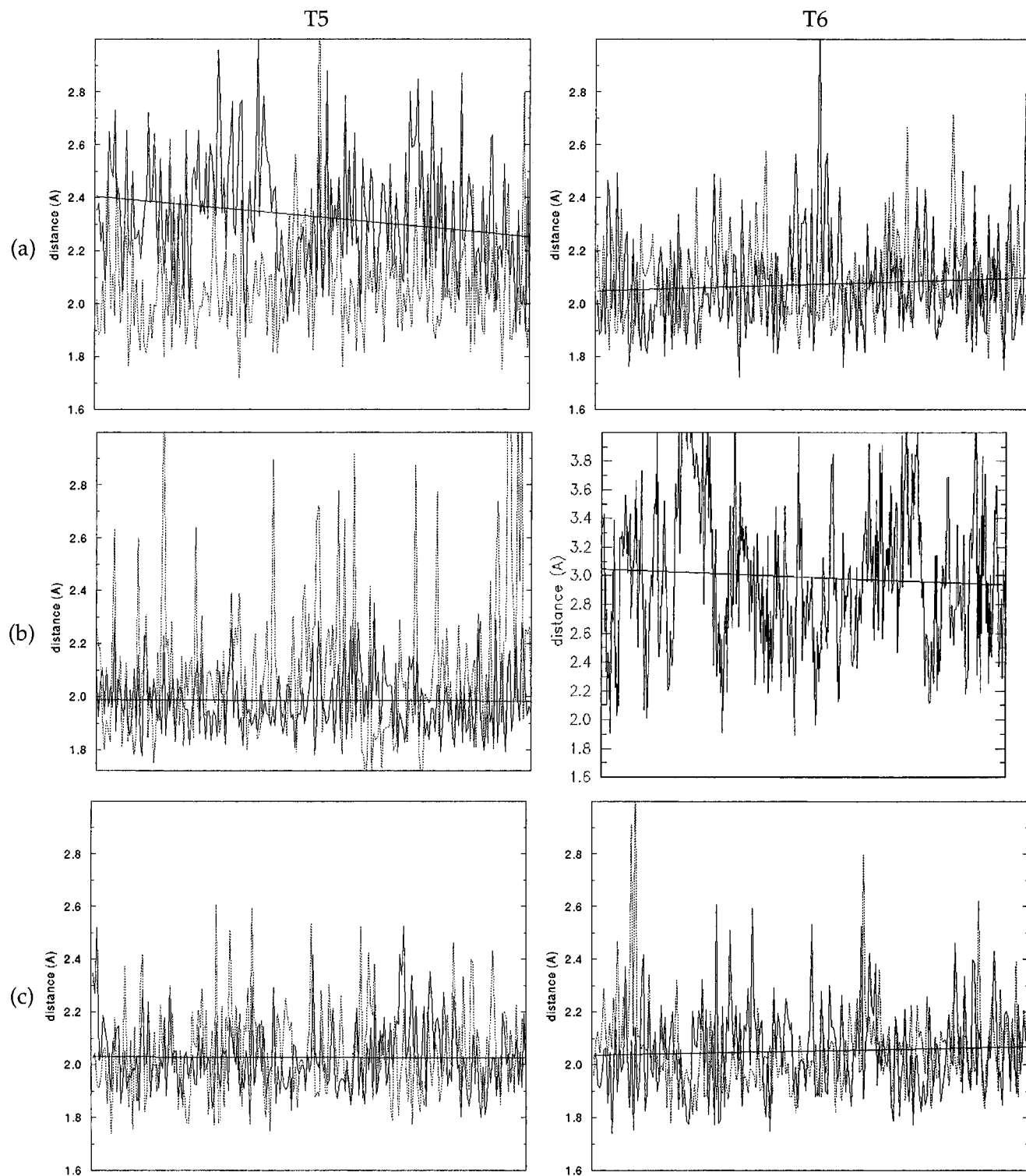


Figure 9. Lengths of hydrogen bonds for the T5-A16 and T6-A15 base pairs of the cis-syn thymine dimer (a), the native duplex (c), and the T5-A16 base pair of the 6-4 pyridine-pyrimidone adduct (b). In each window the H3...N1 (—) and the O4...H61 (···) are shown. The time for the simulation increases from 580 to 800 ps from left to right in each window except for the window for the T6-A15 base pair of b, which depicts only the O2...H61 hydrogen bond length from 800 to 1150 ps. The line across each window indicates the average hydrogen bond length value at each ps.

not have been sufficient to accurately describe those parts of the structure not definitively determined by the NMR data. In our opinion, our simulation methodology¹¹ may offer a powerful complement to NMR determination of nucleic acid structure; since it is significantly more realistic than in vacuo models, one may need far fewer and weaker restraints to both satisfy the NMR data and accurately represent the parts of the structure not well determined by the data. Currently, we are comparing

the duplex structures determined by unrestrained MD for sequences where there is the most accuracy of our simulation model.²⁸

In contrast to the large difference in overall bend in the NMR data and simulated 6-4 adduct, the 7° experimental bending angle of the cyclobutane dimer is similar to our calculated value

(28) Cheatham, T. E.; Konerding, D.; James, T. L.; Kollman, P. A. Work in progress.

Table 8. Local Axis of Curvature Angles (Å) for Each Base Step of **A**, **B**, and **C**^a

duplex	cis-syn dimer (A)	6-4 adduct (B)	control (C)
C1/G2	10.2 ^b	13.8 ^b	4.7
G2/C3	2.1	8.5	5.3
C3/A4	10.0	14.8	10.2
A4/T5	11.6	2.6	2.9
T5/T6	18.3	19.3	2.5
T6/A7	4.3	9.2	7.3
A7/C8	1.1	10.5 ^b	2.3
C8/G9	4.4	5.4	3.9
G9/C10	4.0	4.3	1.9

^a T5 and T6 base step values are in boldface. ^b Non-lesion curvature angles which vary significantly from control **C** values.

(14° relative to the control). Qualitatively, our overall bending angle for the cis-syn system (**A**) also agrees with Taylor and Wang's 7° bend for A-track DNA 21-mers,²⁹ Miaskiewicz *et al.*'s 10° bend for the simulated d(CGCGAATTCGCG)₂ structure,¹² and Rao *et al.*'s in vacuo study of the photodamaged Dickerson dodecamer.⁷

On the basis of our calculations, the overall bending angle is not likely to be the determinant of difference in the repair of photodamaged DNA. Likely, either variances in the local helicoidal parameters from that of control B-DNA or the weakness of the hydrogen bonds at the lesion site (which would ultimately allow the bases to more readily break their Watson–Crick bonds) is the determinant of repair enzyme action. As shown in Table 8, a measure of the relatively large local distortions of the 6-4 adduct relative to the control and cis-syn dimer is the axis curvature of each base step. In addition, as detailed earlier for the torsion, helicoidal, and hydrogen bonding parameters, the substantial differences in **A**, **B**, and **C** are found in the local distortions from helicity for the three decamers. Thus, the control (**C**) has only slight local deviations from helicity relative to canonical B-DNA while the cis-syn dimer (**A**) and 6-4 adduct (**B**) shows significant distortions at the T5–A16 base pair.

Conclusion

Unrestrained PME molecular dynamics calculations has provided, to our knowledge, the first reasonably realistic simulated structure for a 6-4 adduct containing DNA duplex (**B**), as well as a cis-syn dimer containing DNA decamer (**A**) and the control decamer **C** of the same sequence. The results of these simulations yielded structures in very good agreement with experiment.⁵ Specifically, there was good correspondence between our interproton distances, torsional and helicoidal

parameters, and the experimentally determined NOEs and torsion angles of the photodamaged structures.

Coincident with the NMR structures,⁵ our simulations show that the structural impact of both the cis-syn and 6-4 photolisions is localized primarily at, or near, the lesion sites. For the cis-syn containing decamer the most notable distortions relative to the nonphotodamaged control (**C**) were limited to A-DNA-like sugar torsions at T5 and variations in the helicoidal tilt and roll parameters at the lesion site. As expected, the 6-4 adduct displayed greater distortions of the torsions and helicoidal angles at the lesion site than the cis-syn dimer containing decamer. The most significant result of our simulation of the 6-4 photolision containing decamer was the observation of an intact (long) hydrogen bond between the carbonyl oxygen of the T6 pyrimidone and the A15 NH₂ not apparent in the refined NMR structure, but which accounts for the unusual experimental A4(H1')–T6(CH₃) NOE better than the NMR-derived structure.⁵ In addition, there is a dramatic difference between the overall helix bend of our simulated structure (5°) and the NMR-derived structure (44°). Given the limitations of the refinement protocol in the NMR structure, one cannot assess which, if either, overall helix bend is correct. To access the accuracy of either helical bend one could use isotopically enriched bases (e.g. C¹³ for T6–(C2)) in order to more accurately place this carbonyl group in the structure.

Overall, based on the results of this study we can now with some confidence simulate other non-canonical or damaged DNA structures. In our laboratory we plan to extend our PME DNA analyses to DNA–enzyme complexes,⁶ parallel/antiparallel DNA sequences, and to predict the structural impact of the Dewar isomer of the 6-4 adduct³ on a DNA decamer.

Acknowledgment. P.A.K. is grateful to acknowledge research support from the NIH through grant CA-25644. T.I.S. would like to acknowledge research support from the Dean's Office of Arts and Sciences at the University of San Francisco. T.E.C. would like to acknowledge research support as a NIH Biotechnology Training Grant (GM08388) and UCSF Chancellor's Graduate Research Fellow. We also acknowledge the Pittsburgh Supercomputing Center (PSC) (MCA93S 017P) for significant computational resources; the UCSF Computer Graphics Laboratory (RR-1081); Michael Crowley of PSC for parallelizing the PME code on the Cray T3D; Tom Darden for making the PME code available; and Jim Vincent and Ken Merz for the original MPI version of AMBER. We would also like to thank Jennifer Miller, Carlos Simmerling, and Uli Schmitz for helpful discussions.

(29) Taylor, J.-S.; Wang, C. I. *Proc. Natl. Acad. Sci. U.S.A.* **1991**, *88*, 9072–9076.